Magnetism in Polyoxometalates: Anisotropic Exchange Interactions in the Co_3^{II} Moiety of $[Co_3W(D_2O)_2(ZnW_9O_{34})_2]^{12-}$—A Magnetic and Inelastic Neutron Scattering Study

Juan. M. Clemente-Juan,*[a] Eugenio Coronado,[a] Alejandro Gaita-Ariño,[a] Carlos Giménez-Saiz,[a] Grégory Chaboussant,[b] Hans-Ulrich Güdel,*[b] Ramón Burriel,[c] and Hannu Mutka[d]

Abstract: The ground-state properties of a Co_3^{II} moiety encapsulated in a polyoxometalate anion were investigated by combining measurements of specific heat, magnetic susceptibility, and low-temperature magnetization with a detailed inelastic neutron scattering (INS) study on a fully deuterated polycrystalline sample of $Na_{12}[Co_3W(D_2O)_2(ZnW_9O_{34})_2]\cdot 40\,D_2O$ (**Co_3**). The ferromagnetic Co_3O_{14} cluster core consists of three octahedrally oxo-coordinated Co^{II} ions. According to the single-ion anisotropy and spin–orbit coupling of the octahedral Co^{II} ions, the appropriate exchange Hamiltonian to describe the ground-state properties of the **Co_3** spin cluster is anisotropic and is expressed as $\mathscr{H} = -2\Sigma_{\alpha=x,y,z}(J_\alpha^{12}\hat{S}_{1\alpha}\hat{S}_{2\alpha} + J_\alpha^{23}\hat{S}_{2\alpha}\hat{S}_{3\alpha})$, where J_α are the components of the exchange interactions between the Co^{II} ions. To reproduce the INS data, different orientations of the two anisotropic J tensors must be considered, and the following conditions had to be introduced: $J_x^{12} = J_y^{23}$, $J_y^{12} = J_x^{23}$, $J_z^{12} = J_z^{23}$. This result was correlated with the molecular symmetry of the complex. The following set of parameters was obtained: $J_x^{12} = J_y^{23} = 1.37$, $J_y^{12} = J_x^{23} = 0.218$, and $J_z^{12} = J_z^{23} = 1.24$ meV. This set also reproduces in a satisfactory manner the specific heat, susceptibility, and magnetization properties of **Co_3**.

Keywords: anisotropic exchange · cobalt · magnetic properties · neutron diffraction · polyoxometalates

Introduction

Magnetic clusters are currently receiving much attention in areas of research such as molecular chemistry, magnetism, and biochemistry. As they are intermediate between small molecules and the bulk state, they can serve as model systems for in-depth understanding of the magnetic exchange interactions and provide a testing ground for theories.[1] A class of inorganic compounds that provides excellent examples of magnetic clusters are the polyoxometalates.[2, 3] These metal oxo complexes have proved to be especially valuable for the study of magnetic interactions in discrete systems, because many of their diamagnetic structures permit the inclusion of well-isolated magnetic clusters with various nuclearities and definite topologies and geometries.[4] A good example of this capability is provided by complexes obtained from the trivacant Keggin ligands $[XW_9O_{34}]^{n-}$ or Dawson–Wells ligands $[X_2W_{15}O_{56}]^{n-}$ and divalent or trivalent paramagnetic transition-metal ions. Thus, tri- to nonanuclear magnetic clusters can be created. Most of them show ferromagnetic interactions, or a coexistence of ferromagnetic and antiferromagnetic interactions, together with large magnetic anisotropies.[5–15]

Detailed information on these electronic parameters was obtained by using a combination of experimental techniques. Typical thermodynamic methods (magnetic susceptibility, magnetization, specific heat) provided information on the sign and magnitude of the exchange parameters, but were mostly insensitive to their anisotropy. The use of inelastic

[a] Dr. J. M. Clemente-Juan, Dr. E. Coronado, A. Gaita-Ariño, Dr. C. Giménez-Saiz
Instituto de Ciencia Molecular
Universidad de Valencia
Doctor Moliner 50, 46100 Burjassot (Spain)
Fax: (+34) 963864859
E-mail: juan.m.clemente@uv.es

[b] Dr. H.-U. Güdel, Dr. G. Chaboussant
Department of Chemistry and Biochemistry
Universität Bern, Freiestrasse 3, 3000 Bern 9 (Switzerland)
Fax: (+41) 31-6314399
E-mail: hans-ulrich.guedel@iac.unibe.ch

[c] Dr. R. Burriel
Instituto de Ciencia de Materiales de Aragón
CSIC-Universidad de Zaragoza, Plaza San Francisco
50009 Zaragoza (Spain)

[d] Dr. H. Mutka
Institute Laue Langevin, Avenue des Martyrs
B.P. 156, 38042 Grenoble Cedex 9 (France)

  0947-6539/02/0824-5701 $ 20.00+.50/0

neutron scattering (INS) spectroscopy has complemented such information by providing more direct access to the lower energy levels and the corresponding spin functions of the magnetic clusters. In fact, this technique has proved to be a valuable tool for obtaining information on the nature of the exchange interactions, in particular on the parameters connected with the magnetic anisotropy. We have used the above approach to study various Co^{II} polyoxometalate complexes: From the simple Co^{II}_3 moiety embedded in the salt $K_8[Co_2(D_2O)W_{11}O_{39}]\cdot n\,D_2O$ (**Co_2**)[16] to larger magnetic clusters with nuclearities of four ($K_{10}[Co_4(D_2O)_2(PW_9O_{34})_2]\cdot n\,D_2O$, **$Co_4$**),[17–19] five ($Na_{12}[Co_3W(D_2O)_2(CoW_9O_{34})_2]\cdot n\,D_2O$, **$Co_5$**),[20] and nine ($K_{16}[Co_9(OD)_3(D_2O)_6(HPO_4)_2(PW_9O_{34})_3]\cdot n\,D_2O$, **$Co_9$**).[9, 21]

In **Co_2**, one tetrahedral and one octahedral oxo-coordinated Co^{II} site share a common oxygen atom. This complex is of special interest because of the inequivalence of the two Co^{II} ions. While the ground state of the tetrahedral ion can be approximated as spin-only $S = 3/2$, we expect an anisotropic situation with an effective $S = 1/2$ for the ground state of the octahedral partner. Whereas the magnetic susceptibility has been interpreted in terms of a Heisenberg coupling model with an antiferromagnetic interaction, the low-energy pattern derived from INS spectra shows a high anisotropy and can be reproduced by an axial anisotropic exchange.

In **Co_4**, the four Co^{II} ions are octahedrally coordinated and all lie in one plane to form a rhombuslike structure. In this case, the difficulties associated with the exchange topology of the cluster are accentuated by the fact that the exchange interactions are expected to be anisotropic due to the highly anisotropic ground state of octahedral Co^{II}. The overall ferromagnetic nature of the exchange coupling in **Co_4** is derived from the susceptibility. The experimental magnetic data can be well reproduced by an exchange Hamiltonian with purely axial anisotropy, although it does not reproduce the Schottky anomaly of the experimental heat capacity. Considering the INS intensity in addition to energies shows that a purely axial anisotropy is the wrong solution. Here, the real strength of the INS technique becomes manifest. We had to extend the anisotropy range, and with the rhombic anisotropy model we finally obtained a set of parameters that are in agreement with both INS energies and intensities.

The **Co_5** spin cluster is composed of two tetrahedral and three octahedral Co^{II} ions. Thus, the exchange network in the magnetic **Co_5** cluster contains an octahedral–octahedral exchange interaction, which resembles those of the related **Co_4** clusters and the **Co_3** cluster of the present work, and a tetrahedral–octahedral exchange interaction, which resembles that of the **Co_2** spin cluster. In analogy to the chemical construction of high-nuclearity complexes by assembly of smaller molecular fragments, one can build up knowledge about the magnetic properties of large magnetic clusters from the known magnetic properties of smaller subunits. We showed that the additional information on the exchange interactions derived from these simpler subunits, together with the high-resolution INS data on a fully deuterated sample of **Co_5**, allows a detailed description of the low-lying energy levels and exchange parameters of the system. This allowed us to identify the presence of two different exchange pathways having different signs and significant anisotropies. Due to the overparametrization this analysis did not, however, yield the orientation of the anisotropy tensors, which we now report here. The parameters reported in a preliminary study on the title compound[20] should be superseded by the more detailed results presented here.

Finally, in the case of **Co_9** the large number of parameters makes a reasonable analysis of the data impossible without the help of clear ground rules based on simpler systems. This makes the analysis of the title compound especially important.

Results

Crystal and molecular structure of the anion: The structure of the salt $Na_{12}[WCo_3(D_2O)_2(ZnW_9O_{34})_2]\cdot 40\,D_2O$ (**Co_3**) was determined by X-ray crystallography. Crystallographic data and parameters are listed in Table 1. The compound is isomorphous to the Zn analogue $Na_{12}[WZn_3(H_2O)_2(ZnW_9O_{34})_2]\cdot 40\,H_2O$ (**Zn_5**), previously reported by Tourné et al.[11] Like this compound, **Co_3** contains similar β-$[ZnW_9O_{34}]^{12-}$ fragments of the Keggin polyoxometalate $[ZnW_{12}O_{40}]^{6-}$, from which a triad of edge-sharing octahedra has been removed. Two of these fragments encapsulate four coplanar metal atoms in such a way that the latter are octahedrally coordinated in a close-packed arrangement. Two of these four sites are related by an inversion center and surrounded by six oxygen atoms of the $[ZnW_9O_{34}]^{12-}$ fragments. These two sites are each randomly occupied by one W atom and one Co atom. The two other sites remain equivalent and contain two Co atoms surrounded by five oxygen atoms of the $[ZnW_9O_{34}]^{12-}$ fragments and the oxygen atom of a D_2O molecule. Then, the magnetic cluster is defined by three octahedrally coordinated Co atoms, as shown in Figure 1.

Table 1. Crystallographic data for **Co_3**.

formula	$Na_{12}[WCo_3(D_2O)_2(ZnW_9O_{34})_2]\cdot 40\,D_2O$
M	6005.70
T [K]	293(2)
radiation	$Mo_{K\alpha}$ ($\lambda = 0.71069$ Å)
crystal system	monoclinic
space group	$P2_1/c$
Z	2
a [Å]	13.0749(16)
b [Å]	17.817(2)
c [Å]	24.205(3)
β [°]	119.047(6)
V [Å^3]	4929.5(10)
ρ [g cm^{-3}]	4.045
μ [mm^{-1}]	23.212
max/min transmission	0.1284/0.0545
crystal form	prism
crystal size [mm]	$0.30 \times 0.20 \times 0.15$
$2\theta_{max}$ [°]	61.06
reflections	40862
independent reflections	14946
observed reflections [$I > 2\sigma(I)$]	13134
restraints/parameters	285/668
GOF on F^2	1.158
final $R(F)$	0.0597
final $Rw(F^2)$	0.1435
max/min in difference map [e Å^{-3}]	7.652/ – 5.201

0947-6539/02/0824-5702 $ 20.00+.50/0 *Chem. Eur. J.* **2002**, *8*, No. 24

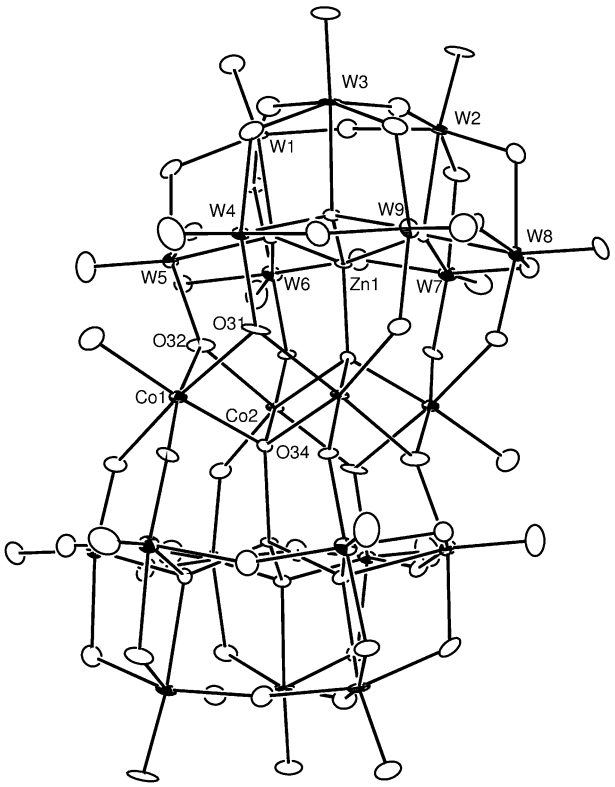

Figure 1. ORTEP plot of the anion of **Co_3** with 60% ellipsoids. For clarity, only crystallographically independent metal atoms and oxo anions involved in the magnetic exchange are labeled. Unlabeled metal atoms are generated by an inversion center. Co2 denotes the random occupancy by W10 or Co2.

The four metal atoms lie at the corners of a rhomboidlike polygon, two opposite sides of which differ slightly in length to the other two (3.170(2) and 3.1827(19) Å). The average Co1-O-Co2 angles, Co1-O-O-Co2 dihedral angles, and Co–O and Co1–Co2 distances are listed in Table 2. For our purposes it is important to note that O31 and O32, though crystallographically independent, are nearly chemically equivalent, so that angles and dihedral angles listed in Table 2 differ by less than 0.4%, and only in the case of the Co–O distances does this value increase to 2%.

Table 2. Average interatomic distances [Å] and bond and dihedral angles [°] in **Co_3**.

Co1-O-Co2 (O31, O32)	96.5
Co1-O-Co2 (O34)	102
Co1-O-O-Co2 (O31–O34, O32–O34)	168.5
Co–O (Co1, Co2; O31, O32, O34)	2.1
Co1–Co2	3.18

Magnetic measurements: Magnetic susceptibility data for a deuterated sample of **Co_3** are shown in Figure 2a, which plots $\chi_m T$ versus T at 0.1, 1, 2, and 4 T. When the sample is cooled from room temperature, $\chi_m T$ decreases from 10.3 emu K mol^{-1} at 293 K to 7.8 emu K mol^{-1} at 35 K, at which a round minimum is observed, then increases at lower temperatures to reach a maximum value at about 6 K (at 0.1 T, see below). The decrease is due to spin–orbit coupling of Co^{II}, while the

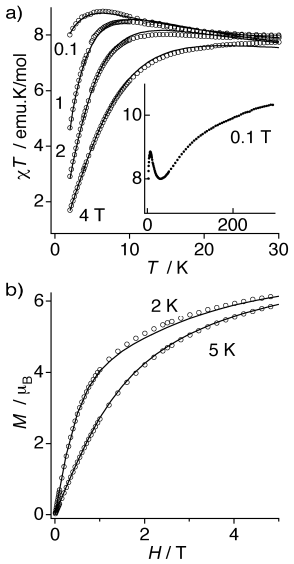

Figure 2. a) Experimental $\chi_m T$ of a polycrystalline sample of **Co_3** between 2 and 30 K (○ at four different fields. Inset: Experimental $\chi_m T$ of the same sample at 0.1 T in the temperature range 2–300 K. b) Isothermal magnetization of **Co_3** at 2 and 5 K. The solid lines represent the magnetic properties calculated by applying the Hamiltonian of Equation (1) with the parameter sets of Equation (2) and a set of g parameters in the usual range.

increase is indicative of ferromagnetic Co^{II}–Co^{II} interactions within the trinuclear spin cluster. The low-temperature behavior (below 50 K) depends on the applied magnetic field. At 0.1 T, $\chi_m T$ reaches a maximum value of 8.8 emu K mol^{-1} at 6 K. At higher fields, the maximum first shifts to higher temperatures and becomes broader and lower, and finally disappears, after which $\chi_m T$ decreases monotonically on cooling. The dependence of the low-temperature isothermal magnetization on field at 2 and 5 K, from 0 to 5 T, is plotted in Figure 2b.

Heat capacity: The results of the heat capacity measurements on **Co_3** and isostructural **Zn_5** are shown in Figure 3a for temperatures below 20 K. They show a smooth behavior with an increasing excess for the magnetic compound on decreasing the temperature. The specific heat of the Zn analogue has the typical T^3 behavior of the lattice contribution at low temperatures, with a Debye constant of $\Theta_D = 200$ K. The curves of the two compounds almost coincide above 30 K. The magnetic contribution of **Co_3** was obtained by subtracting the molar heat capacity of the other compound. The difference shows a Schottky-type anomaly with a maximum at 7 K (Figure 3b). The absolute values of the anomaly were scaled to the maximum height of the Schottky contribution given by the energy levels deduced from the INS measurements. Thus, we take into account the occupational defects (see below).

Inelastic neutron scattering: Figure 4 shows the INS spectra of polycrystalline **Co_3** with an incident neutron wavelength of 4.1 Å at four temperatures. The energy-transfer range between −3.8 and 4 meV is depicted with positive values for neutron-energy loss (right) and negative values for neutron-energy gain (left). The resolution is 110 μeV at the position of the elastic peak. At 1.7 K we observe two inelastic transitions

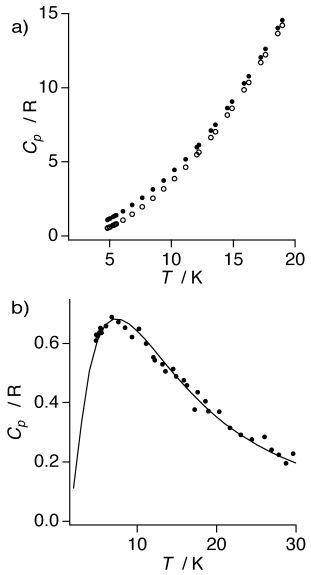

Figure 3. a) Experimental heat capacity data for $\mathbf{Co_3}$ (●) and $\mathbf{Zn_5}$ (○) below 20 K. b) Magnetic heat capacity deduced from the measured values (see text). The solid line is the curve calculated by using the exchange parameters derived from INS.

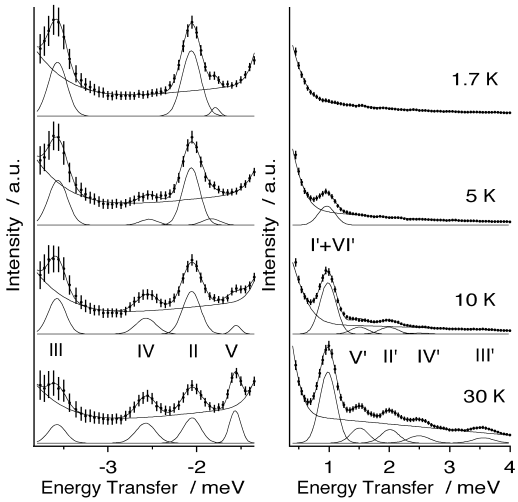

Figure 4. INS spectra of $\mathbf{Co_3}$ at 1.7, 5.0, 10, and 30 K, measured on IN6 of ILL with an incident wavelength of $\lambda = 4.1$ Å. The labels of the transitions are explained in the text. Right: neutron-energy loss side. Left: neutron-energy gain side.

at 2.04 and 3.54 meV on the neutron-energy loss side, labeled II and III, respectively. At 4.1 Å the loss spectrum is obscured below 1 meV by a spurious shoulder, most probably a Bragg reflection of the aluminum-shielded cryostat. On increasing the temperature to 5, 10, and 30 K two hot peaks appear at 2.5 and 1.5 meV, labeled IV and V, respectively. The corresponding gain transitions II′ – V′ (Figure 4, right) appear with rising temperature, as the excited levels become populated. A new transition is observed at 1.0 meV and denoted I′(+VI′). This transition is obscured on the neutron-energy loss side by the spurious peak. On the gain side all five peaks are resolvable, while on the loss side only II – V are resolvable. The least-squares fitting analysis in Figure 4 was performed by assuming one Gaussian for each peak. As background we used the INS spectra of $Na_{12}[Mn_3W(D_2O)_2(ZnW_9O_{34})_2]\cdot 46D_2O$ under the same conditions, as this isostructural compound is silent in this region. The intensities derived from the least-squares fitting analysis are summarized in Table 3.

Figure 5 shows INS spectra of $\mathbf{Co_3}$ at 5.9 Å. At this wavelength, the range between – 1.4 and 1.8 meV is covered, so only the peaks I(+VI) and I′(+VI′) are observed. In this case, the peak I(+VI) is not obscured, and resolution at the elastic-peak position is improved to 40 μeV. At 30 K, we can

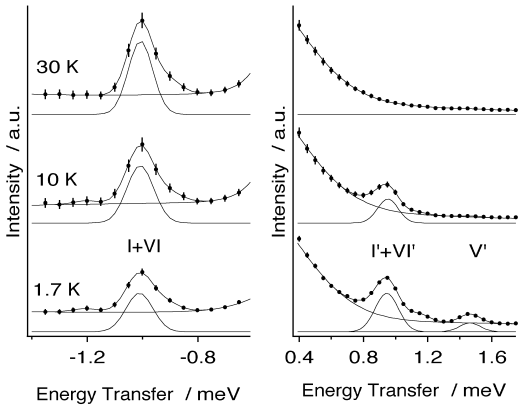

Figure 5. INS spectra of $\mathbf{Co_3}$ recorded at 1.7, 10, and 30 K, measured on IN6 of ILL with an incident wavelength of $\lambda = 5.9$ Å. The labels of the transitions are explained in the text. Right: neutron-energy loss side. Left: neutron-energy gain side.

Table 3. Experimental and theoretical energies and relative intensities of the INS transitions.

	Energy [meV]		Intensity [arbitrary units] 1.5 K		5 K		10 K		30 K		λ	Q range
Label	exptl	calcd	exptl	calcd	exptl	calcd	exptl	calcd	exptl	calcd	[Å]	[Å^{-1}]
I′	0.98(1)	0.98	0	0	0.212(3)	0.0974	0.559(6)	0.276	0.76(2)	0.445	4.1	0.276 – 2.30
V′	1.50(1)	1.50	0	0	0	0	0.080(3)	0.009	0.149(5)	0.086	4.1	0.276 – 2.30
II′	2.040(6)	2.040	0	0	0	0.008	0.083(3)	0.065	0.138(4)	0.190	4.1	0.276 – 2.30
IV′	2.56(1)	2.56	0	0	0	0	0.011(2)	0.009	0.074(3)	0.080	4.1	0.276 – 2.30
III′	3.54(1)	3.54	0	0	0	0	0.005(1)	0.010	0.055(2)	0.088	4.1	0.276 – 2.30
I	– 0.98(1)	– 0.98	–	0.981	–	0.963	–	0.880	–	0.658	4.1	0.276 – 2.30
V	– 1.50(1)	– 1.50	0	0	0.095(8)	0.006	0.18(1)	0.053	0.303(8)	0.155	4.1	0.276 – 2.30
II	– 2.040(6)	– 2.040	1.00(1)	1.000	0.87(1)	0.901	0.70(1)	0.700	0.42(1)	0.419	4.1	0.276 – 2.30
IV	– 2.56(1)	– 2.56	0	0	0.127(8)	0.069	0.30(1)	0.168	0.34(1)	0.214	4.1	0.276 – 2.30
III	– 3.54(1)	– 3.54	0.797(6)	0.830	0.681(6)	0.748	0.493(9)	0.581	0.256(9)	0.347	4.1	0.276 – 2.30
I′	0.980(7)	0.980	–	0	–	–	0.274(6)	0.274	0.494(7)	0.431	5.9	0.192 – 1.599
V′	1.51(1)	1.51	–	0	–	–	0.011(2)	0.008	0.101(3)	0.071	5.9	0.192 – 1.599
I	– 0.980(7)	– 0.980	1.00(2)	1.000	–	–	0.84(2)	0.871	0.57(2)	0.636	5.9	0.192 – 1.599

0947-6539/02/0824-5704 $ 20.00+.50/0 *Chem. Eur. J.* **2002**, *8*, No. 24

also resolve the peak V′. The resulting intensities are also summarized in Table 3.

The good statistics of the spectra allowed the behavior of the scattering intensity of transitions I–V to be studied as a function of the scattering vector Q, at ten intervals (between 0.192 and 1.599 Å^{-1} for $\lambda = 5.9$ Å, and between 0.276 and 2.30 Å^{-1} for $\lambda = 4.1$ Å). Some typical results are plotted in Figure 6 for transitions I and V. The observed Q dependencies identify transitions I–V as magnetic; phonon excitations would typically show an increase of the INS intensity proportional to Q^2.

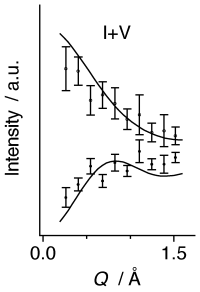

Figure 6. Experimental and calculated Q dependencies of the INS intensities of transitions I + VI and V. The form factors $F(Q)$ are taken from the literature,[36] and the Co–Co distances from the X-ray structure. The intensities of transitions I + VI and V are very different (see Table 3), so they have been scaled.

From the experimental data presented in Figures 4 and 5 and Table 3, we derive the energy-level diagram depicted in Figure 7. The cold transitions I–III originating from the ground level are indicated by full arrows, and hot transitions from the excited levels by broken arrows. The two hot transitions (IV and V) are from the two lower excited states (0.98 and 2.04 meV) to the highest energy level (3.54 meV). Analysis of the temperature dependence of the peak intensities is consistent with a scheme of four energy levels with equal degeneracies and relative energies of 0.00, 0.98, 2.04, and 3.54 meV. According to this energy level diagram, another transition (VI) between the two lower excited states may be observed at 1.06 meV. Such a transition is very close in energy to transition I (0.98 meV), so the peak assigned to I should actually come from these two near-isoenergetic transitions and is denoted I(+VI).

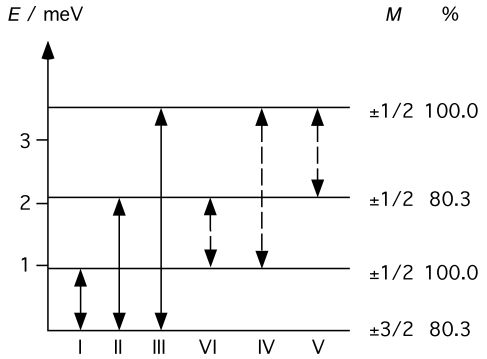

Figure 7. Experimental ground-state splitting. The cold transitions I–III originating in the ground level are shown with full arrows. The hot transitions originating from the excited levels at 0.98 and 2.04 meV are shown with broken arrows. Each gain transition is experimentally observed, and therefore all arrows are double-headed. The neutron-energy gain transitions are referred to in the text as I′, II′, etc. Each energy level is labeled according to the M_s associated with the basis functions having the major contribution in the wave functions Ψ_n of the Co_3^{II} moiety. This contribution, that is, the sum of the squared coefficients in the linear combination in Equation (2), is given on the right.

Discussion

Anisotropic exchange model: Magnetostructural correlations for octahedrally coordinated Co^{II} are far from clear, but due to the small differences in the exchange pathways along the oxo bridges, we can regard the subunit Co_3O_{14} as having idealized C_2 symmetry. It is formed by three edge-sharing CoO_6 octahedra. The two terminal CoO_6 octahedra share nonparallel, noncoplanar edges with the central CoO_6 moiety, and are not connected with each other. The structure is shown in Figure 1. In view of this geometry, the exchange pathways between the central Co^{II} ion and the two terminal ions are equivalent. Furthermore, the lack of bridging atoms between the terminal Co^{II} ions allows us to assume, in a first approximation, that the exchange interaction between these terminal ions is negligible.

The $^4T_1$ high-spin ground state of octahedral Co^{II} shows a first-order spin–orbit coupling and splits into six anisotropic Kramers doublets. At low temperature (below 30 K) only the lowest Kramers doublet is populated, so that the exchange interaction between two Co^{II} ions can be described by assuming a coupling between these fully anisotropic Kramers doublets with effective spins of 1/2. Expressing this spin anisotropy in terms of exchange anisotropy gives the effective exchange Hamiltonian for our Co_3^{II} moiety [Eq. (1)].

$$\mathscr{H} = -2\Sigma_{\alpha=x,y,z}(J_\alpha^{12}\hat{S}_{1\alpha}\hat{S}_{2\alpha} + J_\alpha^{23}\hat{S}_{2\alpha}\hat{S}_{3\alpha}) \quad (1)$$

Generally, the operator involved in Equation (1) does not commute with $\hat{S}^2$, the total spin of the system. Therefore neither S nor M are good quantum numbers of the system, and the eigenfunctions of the trinuclear unit will be given by appropiate linear combinations of the $|\tilde{S}_2)SM\rangle$ basis functions [Eq. (2)]:

$$\Psi_n = \Sigma_{\tilde{S}_2,S,M} a_n(\tilde{S}_2,S,M)\,|(\tilde{S}_2)SM\rangle \quad (2)$$

in which $a_n(\tilde{S},S,M)$ are the eigenvector coefficients of the cluster levels, and $\tilde{S}_2$ is an intermediate spin quantum number, defined as $\tilde{S}_2 = S_1 + S_2$.

The models so far used to successfully reproduce the INS spectra of the closely related systems **Co_4** and **Co_5** required the consideration of fully anisotropic exchange interactions ($J_x \neq J_y \neq J_z$) with parallel J tensors.[15, 16] In fact, an axial exchange model (with $J_x = J_y \neq J_z$) proved to be clearly insufficient for the correct analysis of the data. Bearing in mind these results, we assumed as a first step the same kind of model to treat **Co_3**. This involves as parameters the three components of the exchange interaction J, since $J_\alpha^{12} = J_\alpha^{23}$ ($\alpha = x, y, z$). However, after exploring the whole range of parameters, no solution was found that matches the experimental energy-level diagram. This result shows that new considerations must be taken into account in the present case. However, it does not mean that the Hamiltonian under consideration is inappropriate. In fact, the problem is not the Hamiltonian itself, but the lack of symmetry considerations. Thus, owing to the angular geometry of the complex we considered, in a second step, the possibility of nonparallel anisotropic J tensors. In view of the C_2 symmetry of the Co_3O_{14} unit it is possible to relate the

  0947-6539/02/0824-5705 $ 20.00+.50/0

diagonal components of the anisotropic exchange tensor $\boldsymbol{J}^{12}$ and $\boldsymbol{J}^{23}$. In this particular case and with the purpose of keeping only diagonal components, the local axes of anisotropy were chosen to point towards some of the oxygen atoms of the octahedral site (see Figure 8), and we chose the same

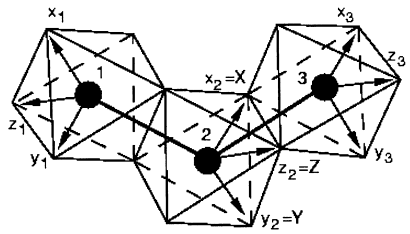

Figure 8. Assumed orientations of the local anisotropy axes, which have been chosen to point towards some of the oxo anions defining the octahedra of each site. The anisotropy axes of 3 and 1 are related by the C_2 symmetry of the molecule. The spatial relations between the anisotropy axes defines the conditions in Equations (1) and (3).

molecular anisotropic tensor as for ion 2. This choice is convenient because then all components of the different local and molecular tensors are parallel or perpendicular to each other. This gives a symmetry-adapted Hamiltonian without nondiagonal exchange components [Eq. (1)], which is not the case if the molecular tensor is chosen to be parallel to the molecular C_2 axis. To some extent, the assumed direction for the anisotropy axes is only an approximation, because it may show some deviations from the coordination axes, as was shown by EPR spectroscopy in simpler systems.[22] However, these studies cannot yet be performed on a relatively complex system like that studied here.

Taking into account the local anisotropic tensors and their projection on the molecular one, we find the following relationship between the parameters: $J_x^{12}=J_y^{23}$, $J_y^{12}=J_x^{23}$, $J_z^{12}=J_z^{23}$. This allows the experimental energy-level scheme depicted in Figure 7 to be reproduced, and the set of parameters given in Equation (3) is obtained.

$$J_x^{12}=J_y^{23}=1.37;\quad J_y^{12}=J_x^{23}=0.218;\quad J_z^{12}=J_z^{23}=1.24\ \text{meV} \tag{3}$$

These parameters imply doubly degenerate levels with linear combination of different $\pm M$ base functions, a level scheme which is typical for axial J anisotropy, but not for a fully rhombic anisotropy. In this particular case, however, the symmetry relations between the exchange components of the two exchange tensors give rise to this surprising energy-level scheme. Table 4 lists the energy of and main contributions to each wavefunction.

To confirm the validity of the proposed solution a full evaluation of the INS transition intensities and Q dependencies was performed. This study should provide direct information on the nature of the eigenfunctions of the trinuclear unit. For this purpose, the relative INS intensities and Q dependencies were analyzed with a general formalism developed in ref. [23] and integrated in the program package MAGPACK.[24] The comparison between experimental and calculated energies and intensities is given in Table 3. For 4.1 Å data the experimental and calculated intensities were scaled to transition II at 1.7 K, which is the most intense transition. For 5.9 Å the most intense transition, I(+VI) at 1.7 K, was normalized to unity. For cold transitions (I – III) the agreement is excellent, and only for excited transitions (IV and V) are the experimental intensities slightly underestimated in the calculated spectra.

Another test is provided by comparison of the experimental and observed Q dependencies of the INS intensities. Figure 6 shows the experimental Q dependencies for two selected transitions in which they are distinctly different and well resolved. The theory closely reproduces these dependencies and confirms the good assignment of the quantum number to each energy level. Thus, the Q dependence for transition I shows a continuous decrease with increasing Q, a behavior typical for a transition between levels with the same S and different M values. In turn, for transition V the intensity increases with increasing Q and reaches a maximum, that is, the initial and final functions of this transition have different values.

Analysis of the magnetic properties: To reproduce the low-temperature magnetic properties, the different g components associated with each center must be taken into account. For this the Zeeman terms are added to the Hamiltonian of Equation (1), and the exchange parameters obtained from the INS analysis are conserved. In a first approximation, the three g tensors were considered to be parallel. No solution was found after exploring the whole range of parameters, with the only limitation $g_i^1=g_i^2=g_i^3$ $(i=x, y, z)$. Hence, a more detailed consideration of the symmetry was again necessary to reproduce the experimental data. A solution was found with an orientation of the g tensors consistent with that assumed for the J tensors [Eq. (4)].

$$g_x^1=g_x^3,\ g_y^1=g_z^3;\ g_z^1=g_y^3;\ g_y^2=g_z^2 \tag{4}$$

This model involves a large number of independent parameters, so to avoid overparametrization, the fit was performed simultaneously over four $\chi_m T$ curves measured at different external magnetic fields (Figure 2a). As the wavefunctions and eigenvalues of the magnetic cluster are accurately determined by INS, the differences observed in

Table 4. Experimental and calculated energy levels with corresponding wavefunctions expanded in the $|(\tilde{S}_2)SM\rangle$ basis obtained by applying the spin Hamiltonian of Equation (1) with the parameter set of Equation (2).

Exptl energy [meV]	Calcd energy [meV]	Main contribution to functions $\lvert(\tilde{S}_2)SM\rangle$
0.00	0.00	$-0.222\,\lvert(0)1/2\mp1/2\rangle-0.384\,\lvert(1)1/2\mp1/2\rangle\pm0.896\,\lvert(1)3/2\pm3/2\rangle$
0.98(1)	0.98(1)	$-0.956\,\lvert(1)3/2\mp1/2\rangle-0.281\,\lvert(1)3/2\pm1/2\rangle$
2.040(6)	2.040(6)	$0.448\,\lvert(0)1/2\pm1/2\rangle+0.776\,\lvert(1)1/2\pm1/2\rangle\mp0.443\,\lvert(1)3/2\mp3/2\rangle$
3.54(1)	3.54(1)	$\mp0.721\,\lvert(0)1/2\mp1/2\rangle+0.475\,\lvert(0)1/2\pm1/2\rangle\mp0.416\,\lvert(1)1/2\mp1/2\rangle-0.274\,\lvert(1)1/2\pm1/2\rangle$

0947-6539/02/0824-5706 $ 20.00+.50/0 Chem. Eur. J. 2002, 8, No. 24

the $\chi_m T$ curves at different magnetic fields can only be due to the Zeeman contributions.

An excellent fit that reproduces the low-temperature range of the $\chi_m T$ measured at different magnetic fields was obtained with the g parameters of Equation (5).

$$g_x^1 = g_x^3 = 6.25;\ g_y^1 = g_z^3 = 4.83;\ g_z^1 = g_y^3 = 0.70;\ g_y^2 = g_z^2 = 4.00 \quad (5)$$

Attention should be paid to the need to introduce anisotropic g values and to the relative orientation of their components, rather than to their values, which can only be taken as approximate.

The validity of the anisotropic exchange model is further confirmed by the low-temperature behavior of the magnetization as a function of the external magnetic field (Figure 2b). The parameters deduced from INS and susceptibility analysis provide an excellent description of the experiment (solid lines in Figure 2). However, the low information content of the magnetic data (χ_m and M), which were obtained from polycrystalline samples, makes it impossible to extract accurate values for the g parameters. Clearly, other combination of parameters can fit the available data equally well, especially if other relative orientations of the g tensors are selected.

Analysis of the specific-heat data: The specific heat gives further independent information that helps to confirm the validity of the model. Assuming the energy levels directly provided by INS (0, 0.98, 2.04, 3.54 meV) are correct, the position and height of the Schottky anomaly can only be properly reproduced by the calculations if all levels have the same degeneracy. Different schemes result in important differences in the shape of the anomaly and/or a shift in its position. As can be seen in Figure 3b, the Schottky anomaly is properly reproduced by using the INS-derived energy-level scheme and the model-derived degeneracy pattern, and this is further experimental support for the model. To quantitatively fit the experimental data, the sample was assumed to contain about 9% of Co-poor polyoxoanions (a mixture of rhomb–side or rhomb–long axis magnetic systems), which would only contribute a small perturbation to the susceptibility and magnetization, and as noisy peaks to the INS experiments, and which are expected from the synthetic pathway.[11]

Conclusion

The ferromagnetic and anisotropic exchange parameters of **Co_3** are in the same range as those of the related compounds **Co_4** and **Co_5**. The small deviations are attributed to the differences in structure and charge distribution due to the substitution of a Co^{II} by a W^{VI} ion (in both **Co_4** and **Co_5**), and of a P^V by a Zn^{II} ion (in **Co_4**).

The current study on the ferromagnetic **Co_3** cluster shows the fruitfulness of paying attention to relatively simple systems. Far from being easier to characterize, this smaller analogue of the **Co_4** and **Co_5** clusters has fairly complex ground-state properties. These two higher nuclearity polyoxometalates, both containing the Co_3O_{14} magnetic network with only minor modifications in bond lengths and angles, have already been successfully studied by INS. These studies yielded a better understanding of the magnetic anisotropy in molecular systems. However, exchange anisotropy, which is significantly caused by single-ion anisotropy, is a very complex phenomenon, and the properties measured on these large clusters may not provide enough information to fully understand it, as they may represent cases of overparametrization. The sign and order of magnitude of the exchange parameters, as well as some indication of their anisotropy, can be extracted from magnetic and other thermodynamic data. The INS spectra are a further step toward providing precise information on the amount of exchange anisotropy. However, in these large clusters INS proved to be insensitive to the relative orientation of the anisotropic J tensors, and a model assuming parallel J tensors was sufficient to reproduce the experiments.

Here we have shown that the symmetry and low nuclearity of **Co_3**, together with the high quality of the INS data, allow a more profound insight into its magnetic anisotropy. For the first time to our knowledge, the different orientation of the anisotropic J tensors had to be taken into account to reproduce the data of a magnetic system. In future this information will be useful for studying in more detail the exchange interactions in higher nuclearity anisotropic magnetic clusters. Further, this result also emphasizes the need to study even simpler systems (i.e., Co_2^{II} moieties) to obtain even better magnetic models in which the nature of the exchange interaction in the presence of orbital degeneracy can be studied by INS. Additionally, theoretical derivation of the appropriate exchange Hamiltonians[25, 26] and calculation of the magnetic parameters[27–31] are required to give a physical meaning to the parameters extracted from an effective and simple spin Hamiltonian. The combination of these three strategies will hopefully lead to a general understanding of magnetic interactions and magnetic anisotropy in molecular clusters formed by anisotropic ions.

Experimental Section

Approximately 15 g of **Co_3** was obtained by the method described in ref. [11]. The last step (metathesis) of the synthesis was performed in D_2O. The deuterated product grew as single crystals, one of which was used for X-ray diffraction. The sample was reduced to fine crystalline powder and sealed under helium in an aluminum container of 15 mm diameter and 55 mm length suitable for INS experiments.

Crystal and molecular structure of the anion of Co_3: Crystals suitable for X-ray diffraction were obtained by repeated crystallization of the sodium salt of the polyoxometalate anion in D_2O. Crystallographic data were collected on a three-circle diffractometer (Bruker Smart CCD) with a CCD detector. Intensities were corrected for Lorentzian and polarization effects. An empirical absorption correction was applied by using the SADABS program based on the Laue symmetry of the reciprocal space. The structure was solved by direct methods (SIR97)[33] and refined against F^2 with a full-matrix least-squares algorithm by using SHELX-97[34] and the WinGX (1.64) software package.[35] Further details of the crystal structure investigation can be obtained from the Fachinformationszentrum Karlsruhe, 76344 Eggenstein-Leopoldshafen, Germany, (fax: (+49) 7247-808-666; e-mail: crysdata@fiz-karlsruhe.de) on quoting the depository number CSD-412572.

Magnetic measurements: Variable-temperature susceptibility measurements were carried out in the temperature range 2–300 K on a 3 mm

  0947-6539/02/0824-5707 $ 20.00+.50/0

diameter compacted pellet molded from a ground crystalline sample of $\mathbf{Co_3}$ on a magnetometer equipped with a SQUID sensor (Quantum Design MPMS-XL-5). The data were corrected for the diamagnetic contribution, which was estimated from the Pascal constants. Isothermal magnetization measurements at low temperature (2 K and 5 K) were performed up to a field of 5 T in the same apparatus.

Inelastic neutron scattering (INS): INS spectra with cold neutrons were recorded on the time-of-flight spectrometer IN6 at the Institut Laue Langevin (ILL) in Grenoble. The measurements were performed at 1.7, 5, 10, and 30 K with an incident neutron wavelength of $\lambda = 4.1$ Å, and at 1.7, 10 and 30 K with $\lambda = 5.9$ Å.

The data processing involved the subtraction of a background spectrum measured on an empty aluminum container of the same size, and calibration of the detectors by means of a spectrum of vanadium metal. Conversion of time-of-flight to energy and data reduction were done with the standard program INX at ILL. The data were treated further by using the commercial program IgorPro 3.14 (Wave Metrics).

Heat capacity: The heat capacity of well-crystallized sample grains was measured in an adiabatic calorimeter[35] from 4.5 to 120 K. 1.5 g of $\mathbf{Co_3}$ was sealed in a 1 cm^3 sample container under 45 mbar of helium gas to ensure heat exchange and temperature equilibration. The measurements were made with temperature steps between 0.5 and 2 K. Carbon – glass and Rh – Fe thermometers were used on the sample holder and on the adiabatic shield that surrounds it, which was held at the temperature of the sample to provide adiabatic conditions. The specific heat of the sample was obtained by subtracting the contribution of the empty sample holder, measured in a separate experiment. Similar measurements were performed on 2 g of isostructural $\mathbf{Zn_5}$ to deduce the specific heat of the nonmagnetic lattice.

Acknowledgement

Financial support by the EU through the TMR program MOLNANOMAG (no. HPRN-CT-1999-0012) is acknowledged. The work in Spain was financed by the Spanish Ministerio de Ciencia y Tecnología and FEDER (MAT 2001-3507) and by the Generalitat Valenciana (GV01 – 312). J.M.C.-J. thanks the Ministerio de Ciencia y Tecnologia for a RyC contract. A.G.A. acknowledges the Generalitat Valenciana for a predoctoral grant.

[1] D. Gatteschi, A. Caneschi, L. Pardi, R. Sessoli, *Science* **1994**, *265*, 1054.
[2] For the state of the art in this area, see *Chem. Rev.* **1998**, *98*, 1 – 390.
[3] M. T. Pope, A. Müller, *Polyoxometalates: From Platonic Solids to Anti-Retroviral Activity*, Kluwer Academic, Dordrecht, **1994**.
[4] J. M. Clemente-Juan, E. Coronado, *Coord. Chem. Rev.* **1999**, *193 – 195*, 361.
[5] C. J. Gómez-García, E. Coronado, L. Ouahab, *Angew. Chem.* **1992**, *104*, 660; *Angew. Chem. Int. Ed. Engl.* **1992**, *31*, 649
[6] C. J. Gómez-García, E. Coronado, J. J. Borrás-Almenar, *Inorg. Chem.* **1992**, *31*, 1667.
[7] N. Casañ-Pastor, J. Bas, E. Coronado, G. Pourroy, L. C. W. Baker, *J. Am. Chem. Soc.* **1992**, *114*, 10380.
[8] C. J. Gómez-García, E. Coronado, P. Gómez-Romero, N. Casañ-Pastor, *Inorg. Chem.* **1993**, *32*, 3378.
[9] J. R. Galán, C. J. Gómez-García, J. J. Borrás-Almenar, E. Coronado, *Adv. Mater.* **1994**, *6*, 221.
[10] J. M. Clemente, E. Coronado, J. R. Galán-Mascarós, C. J. Gómez-García, *Inorg. Chem.* **1999**, *38*, 55.
[11] C. M. Tourné, G. F. Tourné, F. J. Zonnevijlle, *J. Chem. Soc. Dalton. Trans.* **1991**, 143.
[12] R. G. Finke, M. W. Droege, *Inorg. Chem.* **1983**, *22*, 1006.
[13] C. J. Gómez-García, J. J. Borrás-Almenar, E. Coronado, L. Ouahab, *Inorg. Chem.* **1994**, *33*, 4016.
[14] R. G. Finke, M. W. Droege, P. J. Domaille, *Inorg. Chem.* **1987**, *26*, 3886.
[15] T. J. R. Weakly, R. G. Finke, *Inorg. Chem.* **1990**, *29*, 1235.
[16] H. Andres, M. Aebersold, H. U. Güdel, J. M. Clemente-Juan, E. Coronado, H. Büttner, G. Kearly, M. Zolliker, *Chem. Phys. Lett.* **1998**, *289*, 224.
[17] C. J. Gómez-García, E. Coronado, J. J. Borrás-Almenar, M. Aebersold, H. U. Güdel, H. Mutka, *Phys. B*, **1992**, *180 – 181*, 238.
[18] J. M. Clemente-Juan , H. Andres, J. J. Borras-Almenar, E. Coronado, H. U. Güdel, H. Büttner, G. Kearly, *Inorg. Chem.* **2001**, *40*, 1943.
[19] H. Andres, J. M. Clemente-Juan, M. Aebersold, H. U. Güdel, E. Coronado, H. Büttner, G. Kearly, J. Melero, R. Burriel, *J. Am. Chem. Soc.* **1999**, *121*, 10028.
[20] H. Andres, J. M. Clemente-Juan, R. Basler, H. U. Güdel, J. J. Borrás-Almenar, A. Gaita, E. Coronado, H. Büttner, S. Janssen, *Inorg. Chem.* **2001**, *40*, 1943.
[21] T. J. R.Weakley, *J. Chem. Soc. Chem. Commun.* **1984**, 1406.
[22] A. Caneschi, D. Gatteschi, N. Lalioti, R. Sessoli, L. Sorace, V. Tangoulis, A. Vindigni, *Chem. Eur. J.* **2002**, *8*, 286.
[23] J. J. Borrás-Almenar, J. M. Clemente-Juan, E. Coronado, B. S. Tsukerblat, *Inorg. Chem.* **1999**, *38*, 6081.
[24] J. J. Borrás-Almenar, J. M. Clemente-Juan, E. Coronado, B. S. Tsukerblat, *J. Comput. Chem.* **2001**, *22*, 985.
[25] E. Coronado, J. J. Borrás-Almenar, J. M. Clemente-Juan, E. Coronado, A. V. Palii, B. S. Tsukerblat,*J. Phys. Chem.* **1998**, *102*, 200.
[26] E. Coronado, J. J. Borrás-Almenar, J. M. Clemente-Juan, E. Coronado, A. V. Palii, B. S. Tsukerblat, *Chem. Phys.* **2001**, *274*, 131.
[27] C. Jiménez Calzado, J. Fernández Sanz, J. P. Malrieu, F. Illas, *Chem. Phys. Lett.* **1999**, *307*, 102.
[28] D.Muñoz, F. Illas, I. de P. R. Moreira, *Phys. Rev. Lett.* **2000**, *88*, 1579
[29] C. Jiménez Calzado, J. Fernández Sanz, J. P. Malrieu, *J. Chem. Phys.* **2000**, *112*, 5158.
[30] N.Suaud, M.-B. Lepetit, *Phys. Rev B* **2000**, *62*, 402.
[31] N. Suaud, M.-B. Lepetit, *Phys. Rev. Lett.* **2002**, *88*, 56405.
[32] A. Altomare, M. C. Burla, M. Camalli, G. Cascarano, C. Giacovazzo, A. Guagliardi, A. G. G. Moliterni, G. Polidori, R. Spagna, *J. Appl. Crystallogr.* **1999**, *32*, 115.
[33] G. M. Sheldrick, SHELX-97, an integrated system for solving and refining crystal structures from diffraction data, University of Götingen (Germany), **1997**.
[34] L. J. Farrugia, *J. Appl. Crystallogr.* **1999**, *32*, 837.
[35] F. Pavese, V. M. Malyshev, *Adv. Cryog. Eng.* **1994**, *40*, 119.
[36] W. Marshall, S. W. Lovesey, *Theory of Thermal Neutron Scattering*, Oxford University Press, Oxford, **1971**.

Received: June 6, 2002 [F4158]

